Zbynek Heger[1]
Marketa Kominkova[1]
Natalia Cernei[1,2]
Ludmila Krejcova[1]
Pavel Kopel[1,2]
Ondrej Zitka[1,2]
Vojtech Adam[1,2]
Rene Kizek[1,2]

[1]Department of Chemistry and Biochemistry, Faculty of Agronomy, Mendel University in Brno, Brno, Czech Republic
[2]Central European Institute of Technology, Brno University of Technology, Brno, Czech Republic

Received December 2, 2013
Revised May 23, 2014
Accepted August 11, 2014

Research Article

Fluorescence resonance energy transfer between green fluorescent protein and doxorubicin enabled by DNA nanotechnology

DNA nanotechnology is a rapidly growing research area, where DNA may be used for wide range of applications such as construction of nanodevices serving for large scale of diverse purposes. Likewise a panel of various purified fluorescent proteins is investigated for their ability to emit their typical fluorescence spectra under influence of particular excitation. Hence these proteins may form ideal donor molecules for assembly of fluorescence resonance emission transfer (FRET) constructions. To extend the application possibilities of fluorescent proteins, while using DNA nanotechnology, we developed nanoconstruction comprising green fluorescent protein (GFP) bound onto surface of surface active nanomaghemite and functionalized with gold nanoparticles. We took advantage of natural affinity between gold and thiol moieties, which were modified to bind DNA fragment. Finally we enclosed doxorubicin into fullerene cages. Doxorubicin intercalated in DNA fragment bound on the particles and thus we were able to connect these parts together. Because GFP behaved as a donor and doxorubicin as an acceptor using excitation wavelength for GFP (395 nm) in emission wavelength of doxorubicin (590 nm) FRET was observed. This nanoconstruction may serve as a double-labeled transporter of doxorubicin guided by force of external magnetic force owing to the presence of nanomaghemite. Further nanomaghemite offers the possibility of using this technology for thermotherapy.

Keywords:
Fullerene / Intercalation / Maghemite nanoparticles / Surface modification / Thiol modified DNA
DOI 10.1002/elps.201400166

Additional supporting information may be found in the online version of this article at the publisher's web-site

1 Introduction

Area of research including the DNA nanotechnologies is nowadays rapidly developing, because this is provided by the rich structural and functional properties of nucleic acids [1,2]. Different directions in the area of DNA nanotechnologies can be observed, such as utilization of nucleic acids for sensing [3,4], self-assembly of different DNA nanostructures like DNA-origami [5–7], use of DNA fragments for construction of nanodevices [8], development of DNA machines [9], or application of nucleic acids as functional materials for biocomputing [10,11]. Applications of DNA-based nanotechnological systems are currently tested also in nanomedicine, where the development of intracellular autonomous sense-and-treat systems and the use of DNA matrices as drug carry/release systems show large potential [12,13].

The nanoscale materials, for targeted therapy of cancer and other diseases, have become the most productive area in biomedical research field [14,15]. Researches in nanotoxicology have indicated that the pharmacological properties, as well as biodegradability, biocompatibility and nontoxicity are crucial for transporting molecules [16]. In this study, Maghemite nanoparticles showing negligible toxicity and good biocompatibility as discussed previously [17–19]

Correspondence: Dr. Rene Kizek, Department of Chemistry and Biochemistry, Mendel University in Brno, Zemedelska 1, Brno 61300, Czech Republic
E-mail: kizek@sci.muni.cz
Fax: +420-5-4521-2044

Abbreviations: AdT SWV, adsorptive transfer square wave voltammetry; **AuNP**, gold nanoparticle; **FRET**, förster/fluorescence resonance emission transfer; **GFP**, green fluorescent protein; **PMP**, paramagnetic particle

Colour Online: See the article online to view Figs. 1–4 in colour.

were used for functionalization of green fluorescent protein (GFP), representing also negligible health risks [20, 21].

In these perspectives, we aimed to suggest a construction using DNA nanotechnology in the form of thiol modified dsDNA connecting GFP, functionalized with two types of nanoparticles (maghemite and gold), with fullerenes carrying commonly used antineoplastic drug doxorubicin. Herein we report that complex constructed in this manner behave as a labeled paramagnetic nanotransporter, which is able to load doxorubicin and transport the drug to the required location. Moreover, due to connection of two fluorophores as GFP and doxorubicin via thiol modified dsDNA, fluorescence resonance emission transfer (FRET) was observed. FRET also called Förster resonance emission transfer is a photophysical process through which electronically excited donor molecules nonradiatively transfers its excitation energy to an acceptor molecule via a long range dipole–dipole interaction [22–25]. This description is applicable when the two molecules are separated by a distance that is large enough so that the approximation of the molecules as point dipoles is valid [26–28]. The FRET observed by us can be used for a fast confirmation of the presence of this drug in complex through spectral overlap.

2 Materials and methods

2.1 Chemicals and pH measurement

Working solutions like buffers and standard solutions were prepared daily by diluting the stock solutions. Standards and other chemicals were purchased from Sigma-Aldrich (St. Louis, MO, USA) in ACS purity, unless noted otherwise. Washing solutions were prepared in MilliQ water obtained using reverse osmosis equipment Aqual 25 (Aqual, Brno, Czech Republic). The deionized water was further purified using apparatus Direct-Q 3 UV Water Purification System equipped with the UV lamp from Millipore (Billerica, MA, USA). The conductance was established to 18 MΩ/cm. The pH was measured using pH meter WTW inoLab (Weilheim, Germany).

2.2 SDS-PAGE

SDS-PAGE was used for confirmation of the presence of GFP in the sample after FPLC isolation. The 12.5% separation gel was used while the concentration of focussing gel was 5%. The apparatus Maxigel (Biometra, Goettingen, Germany) was used in this case. Separation was conducted under 120 V, until forefront in the gel did not reach down end (~80 min). During separation, the whole space was cooled by water. The gel was stained using Rapid Coomassie Blue staining. After that the gel was heated for 1.5 min till boiling with solution No. 1 (0.05 g Coomassie brilliant blue R250 (CBR-250) dissolved in 25 mL of isopropanol, 10 mL of acetic acid, and 65 mL of H_2O). Subsequently the gel was shaken on Biosan Orbital shaker (Biosan, Riga, Latvia) for 5 min. After shaking, the solution was removed and the gel was washed with water. After that, solution No. 2 (0.005 g CBR-250 dissolved in 10 mL of isopropanol, 10 mL of acetic acid, and 80 mL of H_2O) was added and the gel was heated. The solution was then removed again and the gel was washed with water. Subsequently, solution No. 3 (0.002 g CBR-250 dissolved in 10 mL of acetic acid and 90 mL of H_2O) was added followed by the removal of excess solution and washing with water. Finally, solution No. 4 (10 mL of acetic acid with 90 mL of water) was added and the gel was heated. After this procedure, the solution was removed. For obtaining GFP fluorescent gels images, a Carestream In Vivo Xtreme Imaging System (Carestream Health, Rochester, NY, USA) was used. Fluorescent scans were carried out before staining of gel with Coomassie brilliant blue. Parameters were set as follows: excitation wavelength 480 nm, emission wavelength 535 nm, exposure time 10 s, binning 2 × 2, *f*-stop 1.1, and field of view 10 × 10 cm.

2.3 MALDI-TOF for GFP identification

For further confirmation of the presence of GFP, MALDI-TOF/TOF MS was applied. The experiments were performed using MALDI-TOF/TOF mass spectrometer Bruker Ultraflextreme (Bruker Daltonik, Bremen, Germany) equipped with a laser operating at wavelength of 355 nm with an accelerating voltage of 25 kV, cooled with nitrogen and a maximum energy of 43.2 μJ with repetition rate 2000 Hz in linear and positive mode, and with software FlexControl version 3.4 and FlexAnalysis version 2.2 for data acquisition and processing of mass spectra respectively. α-cyano-4-hydroxycinnamic acid was used as the matrix. The matrix was prepared in TA30 (30% acetonitrile, 0.1% TFA solution, w/w). Working standard solutions were prepared daily by dilution of the stock solutions. The solutions for analysis were mixed in ratio of 1:1 (matrix/substance). After obtaining a homogeneous solution, 1 μL was applied on the target and dried under atmospheric pressure and ambient temperature. A mixture of peptides calibrations standard (Bruker Daltonik) was used for external calibration of the instrument. The MS spectra were acquired by averaging 20 subspectra from a total of 500 shots of the laser (Smartbeam 2. Version: 1_0_38.5).

2.4 Determination of total protein content

The total protein content was determined for results standardization and was performed using SKALAB CBT 600T kit (Skalab, Svitavy, Czech Republic) according to manufacturer instructions. For analysis, BS-400 automated spectrophotometer (Mindray, Schenzhen, China) was used.

2.5 Preparation of nanoparticles

Nanomaghemite particles (MAN32) were prepared according to the following protocol. Briefly, 5 g of $FeCl_3 \cdot 6H_2O$ was dissolved in 400 mL of water and subsequently 1 g of $NaBH_4$

in 50 mL of 3.5% NH_3 (7 mL 25% NH_3 in 43 mL of H_2O (v/v)) was added. Mixture was heated for 2 h at 100°C. After cooling to room temperature nanomaghemite was separated using the magnetic force of external magnetic field. Further, maghemite nanoparticles were washed five times with water and dried at 40ºC. Au nanoparticles were prepared by citrate method at room temperature according to Kimling et al. and Polte et al. [29, 30]. Briefly, an aqueous solution of sodium citrate (0.5 mL, 40 mM) was added to a solution of $HAuCl_4 \cdot 3H_2O$ (10 mL, 1 mM). The color of the solution slowly changed from yellow to violet. The mixture was stirred overnight. Doxorubicin@fullerenes conjugate was prepared according to our previous study [31] in concentration of 500 μg/mL.

2.6 Determination of size distribution and zeta potential

Particle size and zeta potential was evaluated using Particle Size Analyzer (Zetasizer Nano ZS90, Malvern instruments, Malvern, UK) as well as size distribution and zeta potential of entire complex. Prior to measurements the conjugates were incubated at 25°C for 15 min in PBS.

2.7 Chromatographic techniques

For identification of highest GFP@nanomaghemite binding affinity, the ion-exchange liquid chromatography (IELC) with post column derivatization by ninhydrin and the absorbance detector in the VIS range were used in conditions according to our preliminary study [32]. Further, for detection of doxorubicin, high performance liquid chromatography with electrochemical and UV-VIS detection was used in configuration and conditions according to Blazkova et al. [31].

2.8 X-ray fluorescence measurements

X-ray fluorescence element analysis was used to confirm that GFP can establish a nonspecific binding with gold nanoparticles (AuNPs). Gold modified GFP was isolated on surface of paramagnetic particles and washed three times with PBS. Than analyses were carried out on Xepos (SPECTRO analytical instruments, Kleve, Germany) fitted with three detectors: Barkla scatter aluminium oxide, Barkla scatter HOPG, and Compton/secondary molybdenum, respectively. Analyses were conducted in Turbo Quant cuvette method of measurement. The parameters for analysis were as follows: measurement duration 300 s, tube voltage from 24.81 to 47.72 kV, tube current from 0.55 to 1.0 mA, with zero peak at 5000 cps, and vacuum switched off.

2.9 Fluorescence measurements

Further, fluorescence analyses were used to obtain the basic information about GFP behavior after binding to various paramagnetic particles, confirmation of successful doxorubicin conjugation to fullerenes, identification of AuNPs influence of GFP fluorescence and for FRET monitoring. For this purpose multifunctional microplate reader Tecan Infinite 200 PRO (TECAN, Maennedorf, Switzerland) was used. Sample was applied into UV-transparent 96-well microplate with flat bottom Costar® purchased from Corning (NY, USA). The dose per well was 50 μL of sample for all analyzed variants. All measurements were performed at 30°C controlled by Tecan Infinite 200 PRO (TECAN, Switzerland). For the fluorescence measurements of doxorubicin, excitation wavelength was set to 480 nm and the fluorescence scans were carried out within the range from 520 to 850 nm (emission wavelength step size: 5 nm, gain: 100, number of flashes: 5). For GFP fluorescence analyses, excitation wavelength was set to 395 nm and the fluorescence scans were carried out within the range from 430 to 800 nm (emission wavelength step size: 5 nm, gain: 80, number of flashes: 5).

2.10 Absorbance analysis

Absorbance was monitored using multifunctional microplate reader Tecan Infinite 200 PRO (TECAN, Maennedorf, Switzerland). Sample was applied to UV-transparent 96 well microplate with flat bottom Costar® purchased from Corning. In all cases, 50 μL of sample was pipetted into each well. All measurements were performed at 30°C controlled by Tecan Infinite 200 PRO (TECAN) in conditions as follows: wavelengths range 230 to 800 nm, wavelength step size 2 nm, and number of flashes 5.

2.11 Electrochemical measurements

Electrochemical measurements of interaction of fullerene with oligonucleotides were carried out in standard electrochemical cell in three-electrode system with working mercury electrode (HMDE), silver chloride (Ag/AgCl/3 M KCl) reference electrode and auxiliary carbon electrode. All measurements were performed in acetate buffer 0.2 M CH_3COOH + 0.2 M CH_3COONa (pH 5.0) at temperature of 25°C. Samples were deoxygenated by argon (99.99%, 120 s) prior to analysis. Measurements were carried out at 663 VA Stand, 800 Dosino, 846 Dosing Interface (Metrohm, Herissau, Switzerland). Software GPES 4.9 was used for data treatment. For detection of CA signal, adsorptive transfer stripping technique connected with square wave voltammetry (AdT SWV) was applied. The parameters of the electrochemical determination were as follows: initial potential 0 V, end potential −1.85 V, frequency 280 Hz, potential step 0.005 V, and amplitude 0.025 V.

2.12 Descriptive statistics

Mathematical analysis of the data and their graphical interpretation were made using Microsoft Excel®, Microsoft

Word®, and Microsoft PowerPoint®. Results are expressed as mean ± SD unless noted otherwise.

3 Results and discussion

3.1 GFP isolation

In the study using exogenous fluorophores as biolabels, a major challenge is to harvest a sufficient amount of proteins of interest for labeling. GFP is special in the sense that it can readily be isolated from *Escherichia coli* transformants and other mutants [21, 33]. We used pGLO plasmid containing *GFP* gene, arabinose operon *araC*, arabinose-induced promoter araBAD and ampicillin resistance gene *Amp´* (Supporting Information S2). The principle, which states that *AraC* operon could induce *E. coli* pGLO to synthesize GFP, was described previously in few studies [34, 35]. Final selection of bacteria transformed in the right way was based on their ampicillin resistance. After harvesting of positive transformants, GFP was isolated using fast protein liquid chromatography. Confirmation of the presence of the protein was subsequently carried out using MALDI-TOF/TOF MS (Fig. 1A), and SDS-PAGE (Fig. 1B), where typical molecular weight of GFP of 26.9 kDa was observed [36, 37]. That provided us the certainty that we are able to produce GFP in sufficient amount and thus we had strong base for the experiment. Shaner et al. described that expressed GFP is bright enough, providing sufficient signal above autofluorescence for detection and has sufficient photostability to be imaged for the duration of the experiment [21].

3.2 Selection of suitable paramagnetic particles for binding GFP

Our first goal was to find a way how to establish a binding between GFP and different types of paramagnetic particles (PMPs) and thereby make the protein paramagnetic. For this purpose we have carried out an analysis with six types of paramagnetic particles synthesized in different manner as it is mentioned in Supporting Information S1. Paramagnetic particles were prepared as a stock solution consisting of 40 mg of PMPs dissolved in 1000 μL of water with ACS purity using ultrasonic homogenizer SONOPULS mini20 (Bandelin electronic, Berlin, Germany) for 2 min. It was shown that sonication is an essential step in PMPs pretreatment, because the PMPs clusters were disrupted, and hence the functional surface of particles was increased. Then, diluted 50 μL of PMPs was mixed together with 200 μL of PBS prior to further experiments. It was necessary to include washing steps as another part of our workflow process. In our preliminary study dealing with paramagnetic particles, we used Britton-Robinson buffer of pH 2 for protonation of amino acids for binding to PMPs [32]. However it was observed that GFP fluorescence was decreasing in direct proportion with pH, due to protonation, thereby blocking the excited-state proton transfer [38, 39]. Therefore PBS (pH 7) was used for washing and removing of undesired impurities using the magnetic force of a permanent magnet, purchased from Chemagen (Baesweiler, Germany). Subsequently GFP interaction with nanomaghemite was carried out in conditions as it follows: 30 min, 10°C, 1250 rpm using Thermomixer® R (Eppendorf, Hamburg, Germany). After proper isolation, nanomaghemite with GFP was washed with PBS for three times again to remove unbound GFP. In compliance with this protocol, we obtained complex of paramagnetic particles with GFP (hereinafter called GFP@nanomaghemite).

For the purpose of the chromatographic analysis, GFP@nanomaghemite had to be dissolved in 3 M HCl in conditions as it follows: 15 min, 25°C, 1250 rpm in Thermomixer® R (Eppendorf). Dissolved GFP@nanomaghemite was transferred to 96-well evaporation plate Deepwell plate 96 (Eppendorf) and evaporated. For evaporation of dissolved GFP@nanomaghemite the nitrogen blow-down evaporator Ultravap 96 with spiral needles (Porvair Sciences limited, Leatherhead, UK) was used. Finally, the samples were resuspended with dilution buffer and analyzed. Identification of GFP binding affinity was carried out on IELC and the results were evaluated as total sum of amino acids for each type of PMPs (Fig. 1C). As it was obvious, the largest affinity was observed after GFP application on MAN32 particles, where the total concentration of amino acids was of 2200 ~ 200 μM. Disparity in individual PMPs was caused by the modification of nanomaghemite with various substances such as Dowex, Amberlite, etc. (Supporting Information S1). Unlike other particles, MAN32 were formed only by nanomaghemite. From this data, we can conclude that modification of nanomaghemite not only increases the specificity of particles, but also decreases the functional surface of nanomaghemite and thus reduces its binding potential. Therefore we decided to use surface active nanomaghemite that acts as an excellent magnetic carrier due to its well defined stoichiometric structure, single-phase character, and quite uniform size distribution with potential to be easily derivatized to immobilize specific organic molecules in a solution. This information was supported by previous experiments [40, 41].

3.3 GFP functionalization

Although we were able to establish a binding between nanomaghemite and GFP and it was important to obtain information about nanomaghemite influence on protein fluorescence. Figure 1D shows that even though fluorescence of GFP@nanomaghemite was reduced to approximately half of original protein, it still ranks more than 12 000 AU and that was still detectable very easily using our methods. Fluorescence analysis shed light on the underlying process and pointed at the loss of fluorescence resulted from protein adsorption onto PMPs surface [42].

Further, we tested hypothesis that GFP may be spontaneously adsorbed onto AuNPs and thereby functionalization of a protein as a base for binding of dsDNA modified with

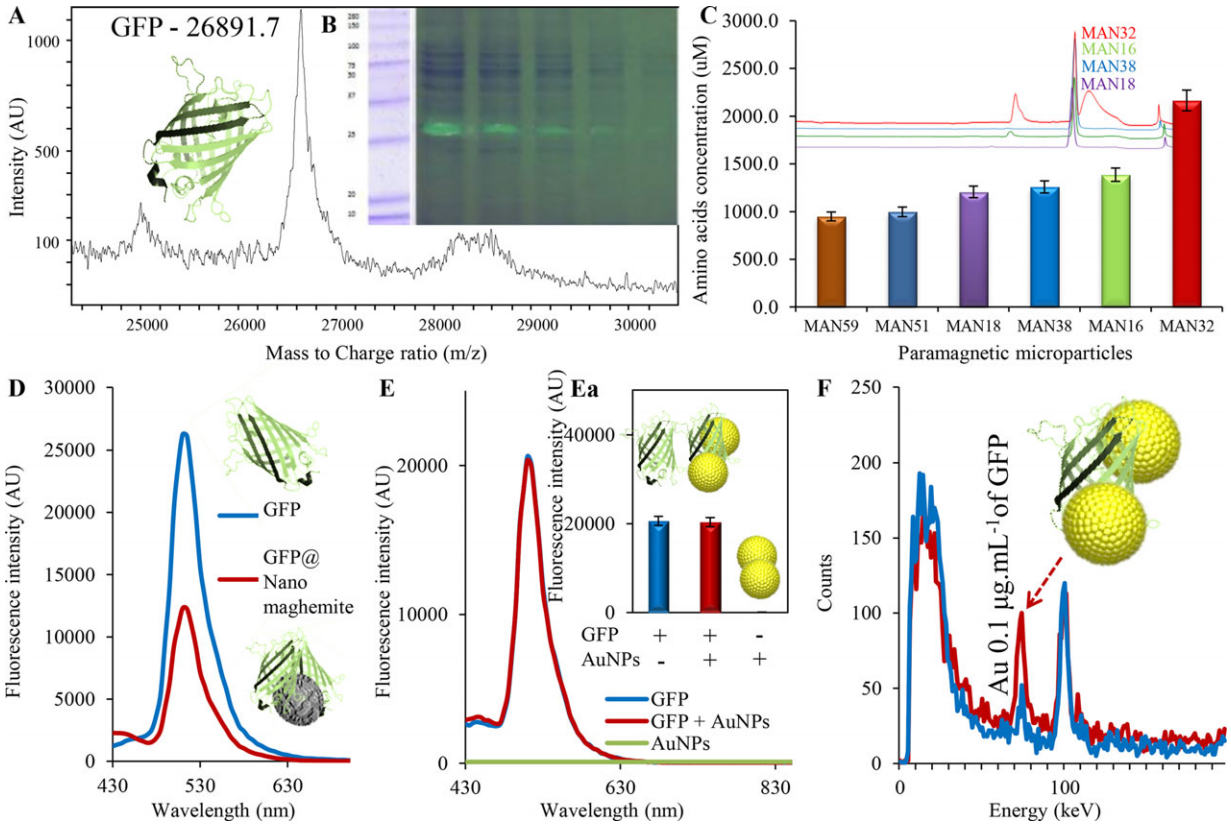

Figure 1. Characterization of green fluorescent protein represented via (A) MALDI-TOF/TOF mass spectra of green fluorescent protein, obtained in conditions as follows: linear positive mode, HCCA matrix used in dry-droplet method. (B) Overlay of SDS-PAGE of GFP (26.9 kDa) stained with Coomassie blue with SDS PAGE without staining, where fluorescence of GFP bands was obtained using fluorescence camera. (C) IELC expression of total amino acids counts bound on different types of paramagnetic particles. (D) Fluorescence spectra of green fluorescent protein compared with green fluorescent protein bind on nanomaghemite (MAN 32), measurements were carried out in following conditions: excitation 410 nm, detector gain 80. (E) Fluorescence spectra of green fluorescent protein and green fluorescent protein in complex with Au nanoparticles. (Ea) Comparison of maxima ($\lambda = 510$ nm) of green fluorescent protein and green fluorescence protein with Au nanoparticles fluorescence (both in concentration of 500 μg/mL). (F) X-ray fluorescence element analysis of green fluorescent protein bind with Au nanoparticles showing the increase of gold in GFP scan after establishing of the GFP/AuNPs complex.

thiol moiety may be carried out and moreover; to serve as a positive control of AuNPs presence prior to doxorubicin intercalation. Bisker and colleagues previously showed that GFP at AuNPs complex may be prepared in a controlled manner using intense single ultrashort pulses with wavelength, tuned to the plasmonic resonance of nanoparticles [42]. Nevertheless their method decreased fluorescence of GFP, probably due to denaturation and aggregation of the protein molecules due to the mechanical and thermal energy released from the irradiated nanoparticles. We used simple procedure for protein attaching to AuNPs comprising mixing of protein in final concentration of 1 mg/mL with AuNPs both dissolved in PBS. The suspension was shaken overnight at 25°C and the resulting solution was filtered using Amicon Ultra Centrifugal Filters with ultracel-3 membrane (Merck Millipore, Darmstadt, Germany) to remove surplus of unbound AuNPs. Similar procedure was used by Bale et al. to form conjugate containing hydrophobic silica nanoparticles and GFP [43]. Immobilized GFP retained 70% of its fluorescence, indicating favorable retention of protein structure after immobilization. Possible conjugation of nanoparticles with GFP with great quantum yield for variety of applications was utilized in many other studies [44–46]. As it can be seen in Fig. 1E and Ea, fluorescence of our GFP with AuNPs conjugate showed only small reduction (20 603 AU for GFP compared to 20 354 AU for conjugate). This phenomenon was probably caused by the low amount of AuNPs conjugated with protein. This statement was subsequently confirmed by X-ray fluorescence analysis, showing that concentration of Au in conjugate after accomplishment of our procedure was 0.1 μg/mL of GFP (Fig. 1F). As it is mentioned in comprehensive review by Love et al. gold binds thiols with a high affinity and it does not undergo any unusual reactions with them [47] and thus only few molecules are required to establish a binding. Demers and colleagues used thiol-modified 12-mer oligonucleotide for AuNPs surface coverage and they concluded that average coverage was approximately 34 ± 1 pmol/cm^2 of AuNPs, corresponding to roughly 159 thiol-bound 12-mer strands per gold particle [48]. While primary purpose of forming conjugate in this manner was to utilize natural ability of gold and

thiol to self-assemble spontaneously, this concentration was sufficient.

3.4 Doxorubicin adsorption on the fullerene cages

After functionalization of GFP, another challenge was to form a construction comprising fullerene cages loaded with doxorubicin, which with its ability to intercalate into dsDNA modified with thiol moieties, created the second fluorophore in our nanotransporter. Currently many researchers are searching for the way how to avoid unwanted serious side effect of doxorubicin, i.e. cardiotoxicity. From this reason, various types of transporters in the form of liposomes [49], apoferritins [50] or fullerenes [31] were developed. In our study, we followed our preliminary findings of using fullerenes as the nanotransporter with perfect ability to carry doxorubicin [31]. Doxorubicin was adsorbed on the C60 fullerene cages in concentration 500 μg/mL. As it can be seen in Fig. 2A, we used HPLC-ED with RP to gain insight into a complex formation. By using this method no signal of pure fullerenes was observed. This phenomenon was caused by the complex structure of especially higher fullerenes that cannot be easily separated and eluted from column [51]. According to the same retention times of doxorubicin and doxorubicin at fullerenes (hereinafter called doxo@fullerenes), we hypothesized that presence of organic mobile phase (acetonitrile in this case) is causing the deconjugation and observed signal belongs to the doxorubicin released from fullerenes. We also determined the influence of doxorubicin adsorption on its fluorescence properties. Adsorption of doxorubicin on fullerenes caused fluorescence quenching (Fig. 2Aa) by approximately 40%, attributed to the strong electron-accepting capability of fullerene [52].

3.5 Confirmation of doxo@fullerenes intercalation into dsDNA

The ability of doxorubicin to intercalate into dsDNA is notorious. It was described previously that there exist two doxorubicin intercalation trajectories [53], but the drug prefers binding between cytosine and guanine bases for the intercalation process [54]. Therefore we suggested ssDNA fragment with the following sequence: 5′ TTGGAATGCAGA 3′ modified with thiol moiety on its 3′ end and we used complementary sequence and hybridization process to obtain functionalized dsDNA containing five cytosine/guanine positions, preferred by doxorubicin as the intercalation sites.

For the basic experiments, we employed the Dynabeads Oligo $(dT)_{25}$ purchased by Invitrogen (Oslo, Norway). These beads provided magnetic properties to our complex and thus we were able to wash unintercalated doxo@fulllerene out of solution and to determine only the actual content of doxorubicin entrapped in dsDNA, which was crucial for the accuracy of analyses. Dynabeads contain magnetic particle caught on the end of tail composed of five thymine bases. For this reason, we performed first hybridization using 5′ TCTGCATTCCAA(AAAAA) 3′ sequence. This sequence was also complementary to our thiol modified DNA, thus, we carried out second hybridization step and finally we obtained magnetic complex of dsDNA with intercalated doxo@fullerene. Procedure of the complex preparation is shown in Supporting Information S3. For complementation of entire transporter, only hybridization of oligonucleotide modified with thiol moieties was carried out to obtain dsDNA(Th).

To gain detailed insight into mechanism of doxo@fullerene intercalation, we performed absorbance analysis, showing that absorbance of doxorubicin (λ_{max} = 485 nm) was reducing from individual doxorubicin, doxo@fullerene to doxo@fullerene intercalated in dsDNA in downward trend (Fig. 2B). Previously it was shown that binding behavior of intercalators is driven almost equally by hydrophobic effect and van der Waals contacts within the intercalation sites [55], whose amounts were capped in our dsDNA. From this reason we did not obtain better doxorubicin yield from ten independent measurements. Nevertheless we received a confirmation that the doxorubicin adsorbed on fullerenes was able to bind with DNA.

Further we employed AdT SWV to explore the complex behavior. Interestingly, we found that AdT SWV, basically used for investigation of biomolecules deposited on hanging mercury drop electrode, may be applied also for measurement of fullerenes or doxorubicin after establishment of binding with DNA (schematically expressed at the top of Fig. 2C). It is obvious from results obtained that doxorubicin has no ability to deposit (adsorb) onto electrode surface as well as fullerenes, which results in no peaks on voltammograms. In contrast to this finding, dsDNA was identified at voltammogram at potential -1.38 ± 0.02 V, corresponding to CA (cytosine–adenine) signal of double-stranded oligonucleotides. After intercalation of individual doxorubicin into dsDNA fragment, the second peak occurred. We still observed CA peak of oligonucleotide, slightly shifted due to interaction with drug (potential -1.54 ± 0.02 V). Moreover we identified also second peak in potential -0.42 ± 0.01 V belongs to doxorubicin. The same situation occurred after interaction with fullerenes. There were also two peaks observed. First CA peak again slightly shifted due to interaction (-1.63 ± 0.02 V) and in potential -0.34 ± 0.01 V, we determined fullerenes peak. Finally, we tested the deposition of dsDNA with intercalated doxo@fullerene. Interestingly three peaks were observed on the voltammogram. The first peak corresponding to fullerene was identified at potential -0.30 ± 0.02 V, second one corresponding to doxorubicin at potential -0.39 ± 0.02 V and the third one as typical CA peak of oligonucleotide in potential -1.64 ± 0.02 V. All peaks were slightly shifted pointing at influence of interactions. As it can be seen in Fig. 2C, peak heights of analytes were converted to percentages for better interpretation. Obviously, peak height of oligonucleotide is decreased after conjugation with doxorubicin, fullerene or doxo@fullerene. Probably analytes compete for a place for adsorption on the electrode surface and thus may affect signals of other compounds.

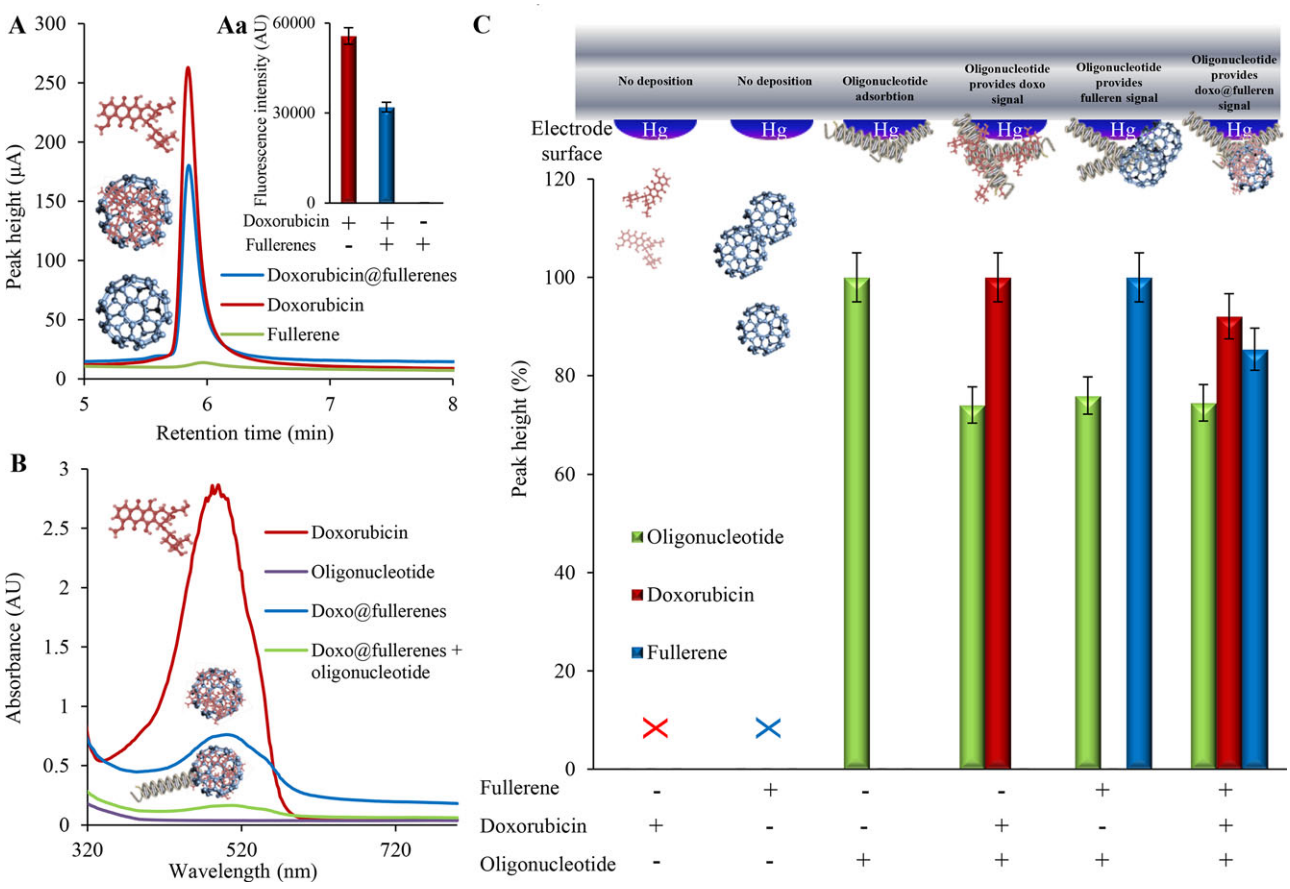

Figure 2. Characterization of doxorubicin presence in fullerenes. (A) HPLC-ED chromatogram of doxorubicin, doxorubicin enclosed in fullerenes and fullerenes without doxorubicin. Concentration of doxorubicin used was 500 μg/mL for both, doxorubicin and doxorubicin@fullerene analysis. (Aa) Comparison of fluorescence maxima (λ = 590 nm) of doxorubicin (20 μg/mL), doxorubicin enclosed in fullerenes and fullerenes without doxorubicin obtained using excitation of 480 nm. (B) Absorption spectra doxorubicin in concentration of 20 μg/mL compared to absorption spectra of doxorubicin enclosed in fullerenes and to absorption spectra of doxorubicin enclosed in fullerenes intercalated into double-stranded oligonucleotide. Last curve represents absorption spectrum of double-stranded oligonucleotide. (C) Electrochemical analysis of interaction between working mercury electrode, oligonucleotide, doxorubicin, fullerenes, doxorubicin@fullerene. In the picture on the top a schematic view of deposition of different substances on the working electrode surface can be seen. Oligonucleotides are only partly able to spontaneously deposit onto electrode surface. After establishment of binding with doxo and fullerenes oligonucleotides may also provide their signal. Below is shown expression of peak height (%) of different substances (fullerene, doxorubicin (20 μg/mL) and oligonucleotide).

3.6 Fluorescence analysis of individual nanotransporter parts

Even though we obtained enough information about functionality of our procedure, we still had not sufficient information about fluorescence behavior of individual nanotransporter parts using both excitation of GFP λ = 395 nm [56] and doxorubicin λ = 480 nm [57]. For this purpose we constructed individual parts of our nanotransporter, shown in Fig. 3. Further, we determined emission maxima belongs to each excitation wavelength (i.e. excitation λ = 395 nm was used to identify GFP emission maximum at 510 nm and excitation λ = 480 nm was used for evaluation of doxorubicin maximum at 590 nm). Results showed that fluorescence intensities of our individual nanotransporter parts were determined as we expected—increasing adsorption of GFP onto paramagnetic particles surface decreased fluorescence as was discussed above as well as only low amount of doxo@fullerene was able to intercalate to dsDNA, which confirmed the absorbance results.

Evaluation of fluorescence of the entire nanotransporter was the most important process for us. To assemble the complementation of construct, we mixed together GFP@nanomaghemite functionalized with AuNPs with doxo@fullerene intercalated to dsDNA. Because we used the principle based on natural affinity of the gold and the thiol moieties interacting together very willingly [47, 58–60], we hypothesized that for anchoring of parts together the interaction for 1 h at 25°C should be sufficient. After interaction in this manner we used force of external magnetic field and removed surplus of liquid, in which doxo@fullerene was applied. Subsequent fluorescence evaluation of entire

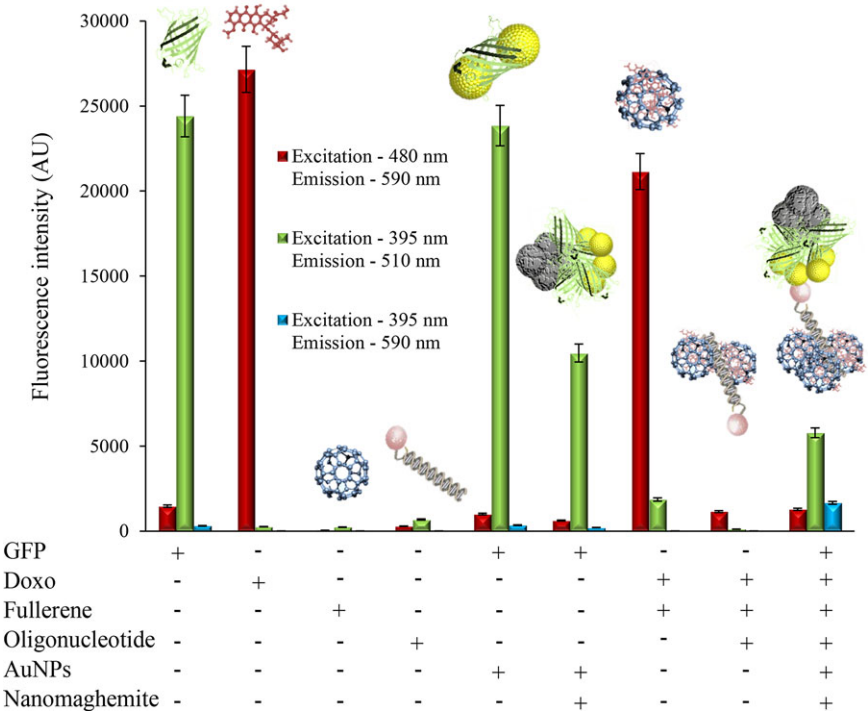

Figure 3. Expression of fluorescence values of individual parts of GFP/doxo@fullerenes complex. Fluorescence analyses were carried out both in excitation wavelength of doxorubicin (480 nm) and green fluorescent protein (500 μg/mL) (395 nm). Subsequent maxima were evaluated in typical wavelengths where doxorubicin and green fluorescent protein showed the largest emission (590 for doxorubicin and 510 nm for GFP). Moreover; FRET mode data (excitation 395 nm with emission 590 nm) are shown.

complex (Fig. 3) showed that according to doxorubicin excitation and emission maxima, nearly all of doxo@fullerene intercalated to dsDNA(Th), self-assembled with AuNPs on GFP@nanomaghemite. When using excitation and emission conditions suitable for GFP, protein fluorescence was observed. That was confirmation for us that both fluorophores are present and thereby we successfully constructed the nanotransporter composed of two fluorophores anchored together with DNA nanotechnology in the form of thiol modified dsDNA. Using a FRET configuration with excitation of 395 nm and emission of 590 nm, significant fluorescence was observed only in case of entire complex (Fig. 3). Hence, it was shown that our construct can assemble a spatial orientation, enabling a spectral overlap between donor—GFP and acceptor—doxorubicin, as it is shown further.

3.7 Förster resonance emission transfer

Since a closed contact of two fluorophores offers a possibility to perform spectral overlap as a result of FRET [61–63], we decided to perform this interaction between GFP and doxorubicin. Anchor, formed by dsDNA(Th), maintained the required proximity for FRET performance, because previously it was found that FRET is enabled only when the distance between two molecules is large enough so that the approximation of the molecules as point dipoles is valid [26, 64] and for the majority of FRET pairs, Förster distance (R_0) values are in the order of a few nanometers (3–7 nm) [65]. The scheme of our nanotransporter is shown in Fig. 4. The basic parameters of entire complex and individual nanoparticles are shown in Table 1. It was shown that entire complex diameter was 151 ± 46 nm (represented only 31% of total analyzed particles, with zeta potential −13.21 ± 3.1 mV). While keeping nanoparticles in blood for sufficiently long time as to allow them to reach their therapeutic target is a major challenge, engineering of the particles morphology, size, and their charge can be one of the factor influencing this requirement [66]. It was shown that particles of less than 10 nm can leave the systemic circulation through the permeable vascular endothelium in lymph node [67]. Ideally, the size of an engineered long-circulatory particle should not exceed 200 nm. If larger, then the particle must be deformable enough to bypass interendothelial cell slits filtration [68].

In Fig. 4 it can be seen that until our two fluorophores were not anchored, they showed their emission maxima in response to their excitation. After anchoring of fluorophores together, spectral overlap was observed, when suitable excitation for GFP was used ($\lambda = 395$ nm) and its fluorescence intensity was decreased (emission at $\lambda = 510$ nm) due to the quenching caused by emission transfer to doxo@fullerene. Hence, doxorubicin was excited with GFP excitation wavelength and emitted photons at its emission wavelength ($\lambda = 590$ nm). This additional ability of our nanotransporter may serve for rapid and cheap confirmation of the presence of doxorubicin. We expect that the entire complex is more sterically complicated than shown in our general disproportional scheme. It does not show the real size of individual components and ODN linkers are probably organized in all directions that causes decrease of donor/acceptor proximity to perform a spectral overlap. As shown in Table 2 FRET efficiency does not change significantly, using various

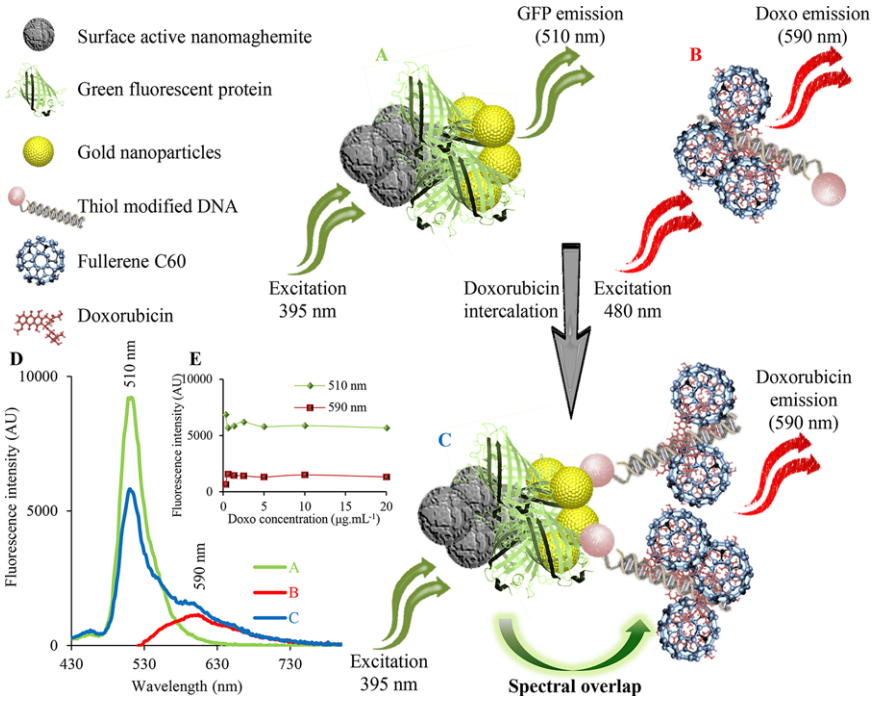

Figure 4. Expression of individual parts of paramagnetic GFP/doxo@fullerenes complex and scheme showing its structure, where GFP@nanomaghemite modified with Au nanoparticles behaves as donor (A) and doxo@fullerenes intercalated into dsDNA fragment modified with thiol moiety as acceptor (B) together able to provide spectral overlap (FRET) (C). Curves showing the shifts of fluorescence caused by FRET are shown in (D). Doxorubicin (concentration applied 0.6 μg/mL) commonly identified at 590 nm using excitation of 480 nm shows fluorescence using excitation of 395 nm—excitation of green fluorescence protein. Moreover; correlation between fluorescence intensities in emission maxima 510 and 590 nm with doxorubicin concentrations in range of 0.3–20 μg/mL is shown in (E).

concentrations of doxorubicin (0.6–20 μg/mL). Amount of doxorubicin determined in construct was in all cases about 0.5 μg/mL (namely 0.48 μg/mL in case where 20 μg/mL of doxorubicin was applied, 0.55 μg/mL in case of 10 μg/mL, 0.48 in case of 5 μg/mL, 0.52 μg/mL in case of 2.5 μg/mL, 0.53 μg/mL in case of 1.3 μg/mL, 0.57 μg/mL in case of 0.6 μg/mL of doxorubicin applied). Decrease in FRET efficiency was observed after application of 0.3 μg/mL of doxorubicin into fullerene cages (0.24 μg/mL of doxorubicin determined). This phenomenon points to a capacity of fullerene nanocages, where limited amount of doxorubicin can be adsorbed, and thus acceptor ability may be evaluated only in the presence of doxorubicin in concentrations higher than approximately 0.2 μg/mL. Utilization of concentrations lower than 0.2 μg/mL cannot provide sufficient spectral overlap, applicable for reliable detection of doxorubicin, as it can be seen in Fig. 4E. However, in doxorubicin concentration range used for experiments (0.3–20 μg/mL), the results

Table 1. The basic characterization parameters of individual nanoparticles including entire complex

Part	Diameter [nm]	Counts [%]	Zeta potential [mV]
Nanomaghemite	37 ± 5	35	−8.12 ± 0.11
AuNPs	15 ± 0.9	58	−19.3 ± 2.14
Fullerene C60	5 ± 0.5	61	−24.6 ± 3.8
Entire complex	151 ± 46	31	−13.21 ± 3.1

Table 2. Expression of FRET efficiency after application of various concentrations of doxorubicin

Concentration of doxorubicin[a] (μg/mL)	Fluorescence (emission 510 nm)[b] (AU)	Fluorescence (emission 590 nm)[b] (AU)	Concentration of doxorubicin determined[c] (μg/mL)	Intraday ($n = 5$)[d] CV (%)	RSD[e] (%)
20.0	5679	1325	0.48	4.25	3.5
10.0	5881	1501	0.55	4.97	4.1
5.0	5799	1315	0.48	6.25	5.2
2.5	6211	1421	0.52	3.26	4.1
1.3	5855	1458	0.53	4.88	3.6
0.6	5674	1567	0.57	6.05	2.5
0.3	6855	658	0.24	5.21	5.1

a) Concentration of doxorubicin used for entrapment into fullerene cage.
b) Excitation wavelength used for measurement 395 nm.
c) Calculation of doxorubicin concentration was carried out according to calibration curve made of fluorescence data in dynamic range of 0.05–50 μg/mL ($y = 0.2815x + 1.0375$).
d) Coefficient of variation
e) RSD for five measurements of the same FRET constructs.

showed relatively good intra-day precision ($n = 5$) within the range 3.26–6.25%, with good RSD of less than 5.2% (Table 2). Since, the core of our complex is constituted by paramagnetic nanoparticles of maghemite, entire complex may be also applied as a recognition element in nanoanalysis via micro-nanofluidic devices. Because of difficulties encountered in ensuring homogeneity and reproducibility of recognition element´s immobilization procedures are crucial for reliable fluidic analyses [69]. Hence, the magnetic nanoparticles, functionalized with various biomolecules—fluorophores in our case, are useful for this purpose, as it was shown previously [70,71]. Therefore, in sense of fluidic device, FRET configuration of our complex, may potentially serve as rapid sensor for the presence of doxorubicin in concentrations higher than 0.2 μg/mL. Unlike other analytical techniques for doxorubicin investigation based on separation like CE or HPLC, FRET is noninvasive, and thus does not disrupt the structure of complex that may be after evaluation of doxorubicin amount further utilized in nanomedicine/theranostics. In these applications, construct offers many other possibilities, where the main role plays drug delivery and its protection against degradation. Importantly, presence of gold nanoparticles imparts the attributes of effective magnetic resonance imaging contrast agent [72], and nanomaghemite, which is labeled by FRET donor GFP, offers possibility to be employed as a labeled photosensitizer in photodynamic therapy [73,74].

4 Concluding remarks

We designed an approach where GFP serves as a doxorubicin nanotransporter's probe providing the paramagnetic properties of entire nanotransporter complex due to functionalization with nanomaghemite. Due to comprehensiveness of our nanotransporter, it meets the conception of the term theranostics—combination of therapeutics and diagnostics. Fluorescent paramagnetic nanotransporter formed in this manner may serve for target transport of doxorubicin into required location. FRET simply feasible between GFP and doxorubicin may serve as a rapid, noninvasive confirmation of the presence of drug. Moreover due to the presence of maghemite nanoparticles, this structure may be applied in cancer thermo and/or photodynamic therapy, employing nanoparticles as the photoabsorbing probes capable of generating reactive oxygen species or heat from optical energy leading to free radicals formation and hyperthermia that can damage the tissues in their vicinity [75–77]. Further magnetic nanoparticles contained in nanotransporter may be utilized also as the vascular contrast agents for magnetic resonance imaging or targeted multimodal imaging [78].

The study was financially supported by CEITEC CZ.1.05/1.1.00/02.0068. The authors wish also to express their special thanks to Dagmar Uhlirova and Lukas Melichar for perfect technical assistance. Moreover, the authors also thank to Dr. Amitava Moulick for critical reading of the manuscript and discussions of our results.

The authors have declared no conflict of interest.

5 References

[1] Aldaye, F. A., Palmer, A. L., Sleiman, H. F., *Science* 2008, *321*, 1795–1799.

[2] Teller, C., Willner, I., *Trends Biotechnol.* 2010, *28*, 619–628.

[3] Huang, P. J. J., Liu, M. C., Liu, J. W., *Rev. Anal. Chem.* 2013, *32*, 77–89.

[4] Kolpashchikov, D. M., *Chem. Rev.* 2010, *110*, 4709–4723.

[5] Wang, F., Willner, B., Willner, I., *Curr. Opin. Biotechnol.* 2013, *24*, 562–574.

[6] Douglas, S. M., Dietz, H., Liedl, T., Hogberg, B., Graf, F., Shih, W. M., *Nature* 2009, *459*, 414–418.

[7] Winfree, E., Liu, F. R., Wenzler, L. A., Seeman, N. C., *Nature* 1998, *394*, 539–544.

[8] Keren, K., Krueger, M., Gilad, R., Ben-Yoseph, G., Sivan, U., Braun, E., *Science* 2002, *297*, 72–75.

[9] Dittmer, W. U., Reuter, A., Simmel, F. C., *Angew. Chem. Int. Ed. Eng.* 2004, *43*, 3550–3553.

[10] Qian, L., Winfree, E., Bruck, J., *Nature* 2011, *475*, 368–372.

[11] Elbaz, J., Wang, F. A., Remacle, F., Willner, I., *Nano Lett.* 2012, *12*, 6049–6054.

[12] Li, D., Song, S. P., Fan, C. H., *Accounts Chem. Res.* 2010, *43*, 631–641.

[13] Douglas, S. M., Bachelet, I., Church, G. M., *Science* 2012, *335*, 831–834.

[14] Shevchenko, E. V., Talapin, D. V., Kotov, N. A., O'Brien, S., Murray, C. B., *Nature* 2006, *439*, 55–59.

[15] Chomoucka, J., Drbohlavova, J., Huska, D., Adam, V., Kizek, R., Hubalek, J., *Pharmacol. Res.* 2010, *62*, 144–149.

[16] Torrano, A. A., Blechinger, J., Osseforth, C., Argyo, C., Reller, A., Bein, T., Michaelis, J., Brauchle, C., *Nanomedicine* 2013, *8*, 1815–1828.

[17] Rudzka, K., Viota, J. L., Munoz-Gamez, J. A., Carazo, A., Ruiz-Extremera, A., Delgado, A. V., *Colloids Surf. B Biointerfaces* 2013, *111*, 88–96.

[18] Wilkinson, K., Ekstrand-Hammarstrom, B., Ahlinder, L., Guldevall, K., Pazik, R., Kepinski, L., Kvashnina, K. O., Butorin, S. M., Brismar, H., Onfelt, B., Osterlund, L., Seisenbaeva, G. A., Kessler, V. G., *Nanoscale* 2012, *4*, 7383–7393.

[19] da Paz, M. C., Santos, M., Santos, C. M. B., da Silva, S. W., de Souza, L. B., Lima, E. C. D., Silva, R. C., Lucci, C. M., Morais, P. C., Azevedo, R. B., Lacava, Z. G. M., *Int. J. Nanomed.* 2012, *7*, 5271–5282.

[20] Richards, H. A., Han, C. T., Hopkins, R. G., Failla, M. L., Ward, W. W., Stewart, C. N., *J. Nutr.* 2003, *133*, 1909–1912.

[21] Shaner, N. C., Steinbach, P. A., Tsien, R. Y., *Nat. Methods* 2005, *2*, 905–909.

[22] Shivkumar, M. A., Adarsh, K. S., Inamdar, S. R., *J. Lumines.* 2013, *143*, 680–686.

[23] Chen, H. Q., Yuan, F., Wang, S. Z., Xu, J., Zhang, Y. Y., Wang, L., *Biosens. Bioelectron.* 2013, *48*, 19–25.

[24] Mizukami, T., Xu, M., Cheng, H., Roder, H., Maki, K., *Protein Sci.* 2013, *22*, 1336–1348.

[25] Erkens, G. B., Hanelt, I., Goudsmits, J. M. H., Slotboom, D. J., van Oijen, A. M., *Nature* 2013, *502*, 119–123.

[26] Kelliher, M. T., Piraino, M. S., Gemoules, M. E., Southern, C. A., *Anal. Biochem.* 2013, *441*, 44–50.

[27] Wang, J. J., Huang, X. Y., Ruan, L. G., Lan, T., Ren, J. C., *Electrophoresis* 2013, *34*, 1764–1771.

[28] Wang, J. J., Huang, X. Y., Zan, F., Guo, C. G., Cao, C. X., Ren, J. C., *Electrophoresis* 2012, *33*, 1987–1995.

[29] Kimling, J., Maier, M., Okenve, B., Kotaidis, V., Ballot, H., Plech, A., *J. Phys. Chem. B* 2006, *110*, 15700–15707.

[30] Polte, J., Ahner, T. T., Delissen, F., Sokolov, S., Emmerling, F., Thunemann, A. F., Kraehnert, R., *J. Am. Chem. Soc.* 2010, *132*, 1296–1301.

[31] Blazkova, I., Nguyen, V. H., Kominkova, M., Konecna, R., Chudobova, D., Krejcova, L., Kopel, P., Hynek, D., Zitka, O., Beklova, M., Adam, V., Kizek, R., *Electrophoresis* 2014, *35*, 1040–1049.

[32] Zitka, O., Cernei, N., Heger, Z., Matousek, M., Kopel, P., Kynicky, J., Masarik, M., Kizek, R., Adam, V., *Electrophoresis* 2013, *34*, 2639–2647.

[33] Zhang, J., Campbell, R. E., Ting, A. Y., Tsien, R. Y., *Nat. Rev. Mol. Cell Biol.* 2002, *3*, 906–918.

[34] Sun, P., Liu, Y., Sha, J., Zhang, Z. Y., Tu, Q., Chen, P., Wang, J. Y., *Biosens. Bioelectron.* 2011, *26*, 1993–1999.

[35] Wong, M., Wright, M., Woodley, J. M., Lye, G. J., *J. Chem. Technol. Biotechnol.* 2009, *84*, 1284–1291.

[36] Feilmeier, B. J., Iseminger, G., Schroeder, D., Webber, H., Phillips, G. J., *J. Bacteriol.* 2000, *182*, 4068–4076.

[37] Niwa, H., Inouye, S., Hirano, T., Matsuno, T., Kojima, S., Kubota, M., Ohashi, M., Tsuji, F. I., *Proc. Natl. Acad. Sci. US A* 1996, *93*, 13617–13622.

[38] Kneen, M., Farinas, J., Li, Y. X., Verkman, A. S., *Biophys. J.* 1998, *74*, 1591–1599.

[39] Haupts, U., Maiti, S., Schwille, P., Webb, W. W., *Proc. Natl. Acad. Sci. USA* 1998, *95*, 13573–13578.

[40] Sinigaglia, G., Magro, M., Miotto, G., Cardillo, S., Agostinelli, E., Zboril, R., Bidollari, E., Vianello, F., *Int. J. Nanomed.* 2012, *7*, 2249–2259.

[41] Magro, M., Faralli, A., Baratella, D., Bertipaglia, I., Giannetti, S., Salviulo, G., Zboril, R., Vianello, F., *Langmuir* 2012, *28*, 15392–15401.

[42] Bisker, G., Minai, L., Yelin, D., *Plasmonics* 2012, *7*, 609–617.

[43] Bale, S. S., Kwon, S. J., Shah, D. A., Banerjee, A., Dordick, J. S., Kane, R. S., *ACS Nano* 2010, *4*, 1493–1500.

[44] De, M., Rana, S., Akpinar, H., Miranda, O. R., Arvizo, R. R., Bunz, U. H. F., Rotello, V. M., *Nat. Chem.* 2009, *1*, 461–465.

[45] Bajaj, A., Rana, S., Miranda, O. R., Yawe, J. C., Jerry, D. J., Bunz, U. H. F., Rotello, V. M., *Chem. Sci.* 2010, *1*, 134–138.

[46] Sanpui, P., Pandey, S. B., Ghosh, S. S., Chattopadhyay, A., *J. Colloid Interface Sci.* 2008, *326*, 129–137.

[47] Love, J. C., Estroff, L. A., Kriebel, J. K., Nuzzo, R. G., Whitesides, G. M., *Chem. Rev.* 2005, *105*, 1103–1169.

[48] Demers, L. M., Mirkin, C. A., Mucic, R. C., Reynolds, R. A., Letsinger, R. L., Elghanian, R., Viswanadham, G., *Anal. Chem.* 2000, *72*, 5535–5541.

[49] Alinaghi, A., Rouini, M. R., Daha, F. J., Moghimi, H. R., *J. Liposome Res.* 2013, *23*, 235–243.

[50] Blazkova, I., Nguyen, H. V., Dostalova, S., Kopel, P., Stanisavljevic, M., Vaculovicova, M., Stiborova, M., Eckschlager, T., Kizek, R., Adam, V., *Int. J. Mol. Sci.* 2013, *14*, 13391–13402.

[51] Yu, Q. W., Shi, Z. G., Lin, B., Wu, Y., Feng, Y. Q., *J. Sep. Sci.* 2006, *29*, 837–843.

[52] Fan, J. Q., Fang, G., Zeng, F., Wang, X. D., Wu, S. Z., *Small* 2013, *9*, 613–621.

[53] Lei, H. X., Wang, X. F., Wu, C., *J. Mol. Graph.* 2012, *38*, 279–289.

[54] Zeman, S. M., Phillips, D. R., Crothers, D. M., *Proc. Natl. Acad. Sci. USA* 1998, *95*, 11561–11565.

[55] Ren, J. S., Jenkins, T. C., Chaires, J. B., *Biochemistry* 2000, *39*, 8439–8447.

[56] Grigorenko, B. L., Nemukhin, A. V., Polyakov, I. V., Morozov, D. I., Krylov, A. I., *J. Am. Chem. Soc.* 2013, *135*, 11541–11549.

[57] Dai, Y. L., Ma, P. A., Cheng, Z. Y., Kang, X. J., Zhang, X., Hou, Z. Y., Li, C. X., Yang, D. M., Zhai, X. F., Lin, J., *ACS Nano* 2012, *6*, 3327–3338.

[58] Hegner, M., Wagner, P., Semenza, G., *FEBS Lett.* 1993, *336*, 452–456.

[59] Sperling, R. A., Parak, W. J., *Ther. Innov. Regul. Sci.* 2013, *47*, 1333–1383.

[60] Frederix, F., Bonroy, K., Laureyn, W., Reekmans, G., Campitelli, A., Dehaen, W., Maes, G., *Langmuir* 2003, *19*, 4351–4357.

[61] Paul, B. K., Ganguly, A., Karmakar, S., Guchhait, N., *J. Lumines.* 2013, *143*, 374–381.

[62] Hu, B., Hu, L. L., Chen, M. L., Wang, J. H., *Biosens. Bioelectron.* 2013, *49*, 499–505.

[63] Du, F. K., Ming, Y. H., Zeng, F., Yu, C. M., Wu, S. Z., *Nanotechnology* 2013, *24*, 1–6.

[64] Dinant, C., Van Royen, M. E., Vermeulen, W., Houtsmuller, A. B., *J. Microsc.* 2008, *231*, 97–104.

[65] Sun, Y. S., Rombola, C., Jyothikumar, V., Periasamy, A., *Cytom. Part A* 2013, *83*, 780–793.

[66] Yoo, J. W., Chambers, E., Mitragotri, S., *Curr. Pharm. Des.* 2010, *16*, 2298–2307.

[67] Moghimi, S. M., Hunter, A. C., Murray, J. C., *Pharmacol. Rev.* 2001, *53*, 283–318.

[68] Moghimi, S. M., Porter, C. J. H., Muir, I. S., Illum, L., Davis, S. S., *Biochem. Biophys. Res. Commun.* 1991, *177*, 861–866.

[69] Diao, J. P., Ren, D. C., Engstrom, J. R., Lee, K. H., *Anal. Biochem.* 2005, *343*, 322–328.

[70] Khun, K., Ibupoto, Z. H., Lu, J., AlSalhi, M. S., Atif, M., Ansari, A. A., Willander, M., *Sens. Actuator B-Chem.* 2012, *173*, 698–703.

[71] Lu, A. H., Salabas, E. L., Schuth, F., *Angew. Chem. Int. Ed. Engl.* 2007, *46*, 1222–1244.

[72] Miladi, I., Alric, C., Dufort, S., Mowat, P., Dutour, A., Mandon, C., Laurent, G., Brauer-Krisch, E., Herath, N., Coll, J. L., Dutreix, M., Lux, F., Bazzi, R., Billotey, C., Janier, M., Perriat, P., Le Duc, G., Roux, S., Tillement, O., *Small* 2014, *10*, 1116–1124.

[73] Ling, D., Park, W., Park, S. J., Lu, Y., Kim, K. S., Hackett, M. J., Kim, B. H., Yim, H., Jeon, Y. S., Na, K., Hyeon, T., *J. Am. Chem. Soc.* 2014, *136*, 5647–5655.

[74] Li, M. H., Deng, H. B., Peng, H. S., Wang, Q., *J. Nanosci. Nanotechnol.* 2014, *14*, 415–432.

[75] Kim, J., Park, S., Lee, J. E., Jin, S. M., Lee, J. H., Lee, I. S., Yang, I., Kim, J. S., Kim, S. K., Cho, M. H., Hyeon, T., *Angew. Chem. Int. Ed. Engl.* 2006, *45*, 7754–7758.

[76] Cheng, L., Yang, K., Li, Y. G., Zeng, X., Shao, M. W., Lee, S. T., Liu, Z., *Biomaterials* 2012, *33*, 2215–2222.

[77] Meffre, A., Mehdaoui, B., Kelsen, V., Fazzini, P. F., Carrey, J., Lachaize, S., Respaud, M., Chaudret, B., *Nano Lett.* 2012, *12*, 4722–4728.

[78] Lee, N., Hyeon, T., *Chem. Soc. Rev.* 2012, *41*, 2575–2589.

